Temperature-dependent nonlinear behaviour of thin rectangular plates exposed to through-depth thermal gradients

Temperature-dependent nonlinear behaviour of thin rectangular plates exposed to through-depth thermal gradients

P. Khazaeinejad[a,*], A.S. Usmani[a], O. Laghrouche[b]

[a] *School of Engineering, The University of Edinburgh, The King's Buildings, Edinburgh EH9 3JL, UK*
[b] *Institute for Infrastructure and Environment, Heriot-Watt University, Edinburgh EH14 4AS, UK*

Abstract

A theoretical model is developed for geometrically and materially nonlinear analysis of thin rectangular plates subjected to transverse mechanical loads and exposed to non-uniform thermal gradients over their depth. The geometrical nonlinearity is based on the von Kármán type of large deformation theory. The material nonlinearity arises from degradable material behaviour at elevated temperatures. The temperature distribution is obtained numerically for two common types of fire exposure conditions that could occur in a fire compartment including: an exponential "short hot" fire leading to a high temperature over a relatively short duration; and an exponential "long cool" fire of lower temperature over a longer duration. Two types of support conditions are considered for the plate based on assuming that in-plane displacements are either restrained or unrestrained against lateral translation. Several numerical examples including two examples for functionally graded plates are presented to assess the accuracy and performance of the proposed method. The evolution of the true shape of the compressive zone supporting tensile membrane action in laterally unrestrained plates under large displacements is graphically illustrated for the two non-uniform thermal gradients. It is shown that the effect of the short hot fire on the plate behaviour is more pronounced.

Keywords: Geometric nonlinearity, Temperature-dependent material properties, Rectangular plate, Non-uniform thermal gradient, Structures in fire, Compressive ring

*Corresponding author. Tel.: +44 (0) 131 650 5806.
Email address: p.khazaeinejad@ed.ac.uk (P. Khazaeinejad)

1. Introduction

In most engineering structures, there are circumstances where structural components are exposed to non-uniform thermal gradients while externally loaded, e.g., when oil platforms or large compartments in buildings are subjected to fire conditions, or when aerospace vehicles are subjected to aerodynamic heating upon reentry into earth atmosphere. Such loading conditions typically induce two effects on the structure, deformation or geometry change (due to thermal expansion) and reduction of strength and stiffness of the structure (due to material degradation). As a consequence, there are two concurrent actions associated with thermally-induced displacements and load-induced displacements. At an early stage of thermal exposure, the structural behaviour is dominated by the latter, however, close to structure failure when material properties have significantly degraded, it is dominated by the former. Such a mechanism was proposed by Usmani et al. [1] to explain how and why the Twin Towers of the World Trade Center in New York collapsed as a result of the terrorist attack. However, full exploitation of the new understanding developed from that research requires further more detailed investigations, so it could lead to designing safer structures.

Considering the complexity of such problems, recourse is made to numerical techniques. Barut et al. [2] presented a nonlinear finite element (FE) formulation for moderately thick flat and curved laminated panels subjected to non-uniform thermal loading over the panel surface and across its thickness. The material properties were assumed independent of the temperature change. The principle of virtual work, along with the co-rotational form of the total Lagrangian formulation were used to derive the governing equations. Jin et al. [3] performed an FE investigation of thermal post-buckling behaviour for patched cylindrical composite panels under uniform and non-uniform temperature distributions through the thickness direction. Their analysis was based on the Hellinger-Reissner principle. Na and Kim [4] studied the nonlinear bending of laterally restrained plates made of functionally graded materials (FGMs) subjected to uniform pressure and thermal loads using a 3D FE method. The thermal loads were assumed to be uniform, linear and quarter sine wave temperature distributions across the plate thickness. Sabik and Kreja [5] numerically investigated the load capacity of

thermally loaded multi-layered plates and shells under uniform thermal loading. Their formulation was based on the first order shear deformation theory, but the thermal degradation of material properties was not taken into account in their model. Another FE analysis was recently performed by Jeyaraj [6] to study the critical buckling temperature and free vibration modes of isotropic plates under arbitrary varying temperature fields. More recently, Salminen and Heinisuo [7] proposed a design method for predicting shear resistance of thin steel plates at non-uniform elevated temperatures. Nonlinear behaviour of steel at elevated temperatures was considered in their model according to Eurocode [8].

Along with advances in numerical methods, a significant improvement is also observed in the capability of analytical and semi-analytical approaches in capturing large deformations of plates and shells. Shukla and Nath [9] used an analytical technique to investigate the steady-state response of moderately thick laminated composite rectangular plates under various boundary conditions (BCs), including simply supported immovable edges, clamped immovable edges, free edges, and their combinations undergoing moderately large deformations. The method of solution was based on a Chebyshev series solution technique. Woo and Meguid [10] studied the nonlinear analysis of laterally unrestrained thin rectangular plates and shallow shells with FGM properties subjected to a transverse mechanical load and a temperature field through the thickness direction. The governing equations were established based on the von Kármán theory for large transverse deflections and were solved using series solutions. Shen [11] presented an analytical method for thermal post-buckling analysis of a simply supported shear deformable functionally graded (FG) plate under both in-plane non-uniform parabolic temperature distribution and heat conduction based on a higher-order shear deformation plate theory. Li et al. [12] analytically studied the geometrically nonlinear deformation of clamped imperfect circular FG plates subjected to both mechanical load and non-uniform temperature increase over the depth of the plate. Recently, Sepahi et al. [13] investigated the effects of thermal and combined thermo-mechanical loadings on axisymmetric large deflection of a simply supported annular FG plate resting on an elastic foundation. The thermal loading was assumed to be non-uniform over the depth of the plate.

In a general sense, numerical methods have been widely adopted by the scientific community to cope with both geometrical and material nonlinearities in thermo-mechanical modelling of plate and shell structures. There is no doubt that such methods provide greater flexibility in analysing structures when compared to closed form analytical methods. It is nevertheless possible to benefit from adequately accurate analytical or semi-analytical approaches that take into account all the key features and complexities of the problem, when computational effort (mostly in terms of analyst effort) is a concern, or when an alternative approach is required to validate and corroborate numerical results. These approaches not only provide rapid alternatives and benchmark solutions for assessing the accuracy and validity of numerical results, they could potentially also provide advanced basis functions for hybrid-type computational approaches. For example, in the context of structures in fire, benchmark solutions can identify interesting interactions between heated structural members and the cooler surrounding structure which sometimes result in sudden changes that are difficult to model numerically.

The application of this concept to various composite structures seems straightforward, however, little work exists in this area. We aim to apply this strategy to plate structures under more realistic thermal loading conditions by simulating extreme thermo-mechanical loads such as fire, through an ongoing research project at the University of Edinburgh in the UK [14, 15]. In most composite plate analyses, particularly for analysis of FG plates, spatially varying material properties are not employed and the analysis has been limited to temperature sensitive material properties.

Hence in this paper, the nonlinear structural behaviour of temperature-dependent rectangular plates subjected to transverse mechanical loads and non-uniform thermal loads is modelled. The thermal loading includes two different fire conditions, one representing a "short hot" exponential fire of high temperature over a short post-flashover duration, while the other represents a "long cool" exponential fire with lower maximum temperature over a longer post-flashover period. Both geometrical and material nonlinearities are included in the model. The geometrical nonlinearity is based on the von Kármán type of large deformation theory, while the material nonlinearity arises from considering the reduction of the plate's mechanical and thermal properties at elevated

temperatures. BCs are such that rotations parallel to the plate boundaries are assumed to be free while lateral translations across the boundaries may be free or restrained. The out-of-plane (or transverse) displacement at the plate boundaries is always restrained. The analysis is carried out assuming quasi-static conditions ignoring any dynamic effect. The difference between the two limiting cases (rigid restraint or zero restraint) under thermal loadings on the plate response is highlighted in the results section. In the case of laterally unrestrained plates undergoing large displacements, the evolution of the shape of the compressive zone supporting tensile membrane action (TMA) is graphically illustrated for the two non-uniform thermal gradients while also considering nonlinear temperature-dependent material behaviour. The accuracy of the present method is investigated through several numerical examples, including two examples for FG plates.

2. Fundamental relations

A rectangular plate of length a, width b, and uniform thickness h subjected to a transverse mechanical load and a non-uniform thermal gradient caused by a heat source across the thickness of the plate is considered as illustrated in Figure 1, where the Cartesian coordinates system (x, y, z) is set on the middle surface of the plate. The plate experiences large displacements which requires using appropriate strain definitions, including mechanical and thermal strains. The former is caused by stress resulting from external loads or restraint to thermal expansion and the latter is caused by thermal expansion. The expressions for the mechanical strains at any point on the plate considering the von Kármán type of geometric nonlinearity, consistent with small strains, moderate rotations, and large displacements, are written as

$$\begin{Bmatrix} \varepsilon_{xx}^{m} \\ \varepsilon_{yy}^{m} \\ \gamma_{xy}^{m} \end{Bmatrix} = \begin{Bmatrix} \frac{\partial u}{\partial x} + \frac{1}{2}\left(\frac{\partial w}{\partial x}\right)^2 \\ \frac{\partial v}{\partial y} + \frac{1}{2}\left(\frac{\partial w}{\partial y}\right)^2 \\ \frac{\partial u}{\partial y} + \frac{\partial v}{\partial x} + \frac{\partial w}{\partial x}\frac{\partial w}{\partial y} \end{Bmatrix} + z \begin{Bmatrix} -\frac{\partial^2 w}{\partial x^2} \\ -\frac{\partial^2 w}{\partial y^2} \\ -2\frac{\partial^2 w}{\partial x \partial y} \end{Bmatrix} \tag{1}$$

where superscript m denotes the mechanical strains and u, v, and w are the middle surface displacements in the x, y, and z directions, respectively, as shown in Figure 1. In

most structural materials, the thermally induced strains due to heating may be obtained by

$$\begin{Bmatrix} \varepsilon^{\theta}_{xx} \\ \varepsilon^{\theta}_{yy} \\ \gamma^{\theta}_{xy} \end{Bmatrix} = \begin{Bmatrix} \alpha_{xx}(\theta, z) \\ \alpha_{yy}(\theta, z) \\ \alpha_{xy}(\theta, z) \end{Bmatrix} \theta(z) \tag{2}$$

where superscript θ denotes the thermal strains, α_{xx}, α_{yy}, and α_{xy} are the temperature-dependent transformed coefficients of thermal expansion and $\theta(z)$ represents the temperature increase through the depth of the plate.

Further normal and shear stresses are integrated with respect to the thickness of the plate to express the force and moment resultants

$$\begin{aligned} \begin{Bmatrix} N_{xx} \\ N_{yy} \\ N_{xy} \end{Bmatrix} &= \begin{bmatrix} A_{11} & A_{12} & A_{16} \\ A_{12} & A_{22} & A_{26} \\ A_{16} & A_{26} & A_{66} \end{bmatrix} \begin{Bmatrix} \frac{\partial u}{\partial x} + \frac{1}{2}\left(\frac{\partial w}{\partial x}\right)^2 \\ \frac{\partial v}{\partial y} + \frac{1}{2}\left(\frac{\partial w}{\partial y}\right)^2 \\ \frac{\partial u}{\partial y} + \frac{\partial v}{\partial x} + \frac{\partial w}{\partial x}\frac{\partial w}{\partial y} \end{Bmatrix} \\ &+ \begin{bmatrix} B_{11} & B_{12} & B_{16} \\ B_{12} & B_{22} & B_{26} \\ B_{16} & B_{26} & B_{66} \end{bmatrix} \begin{Bmatrix} -\frac{\partial^2 w}{\partial x^2} \\ -\frac{\partial^2 w}{\partial y^2} \\ -2\frac{\partial^2 w}{\partial x \partial y} \end{Bmatrix} - \begin{Bmatrix} N^{\theta}_{xx} \\ N^{\theta}_{yy} \\ N^{\theta}_{xy} \end{Bmatrix} \end{aligned} \tag{3}$$

$$\begin{aligned} \begin{Bmatrix} M_{xx} \\ M_{yy} \\ M_{xy} \end{Bmatrix} &= \begin{bmatrix} B_{11} & B_{12} & B_{16} \\ B_{12} & B_{22} & B_{26} \\ B_{16} & B_{26} & B_{66} \end{bmatrix} \begin{Bmatrix} \frac{\partial u}{\partial x} + \frac{1}{2}\left(\frac{\partial w}{\partial x}\right)^2 \\ \frac{\partial v}{\partial y} + \frac{1}{2}\left(\frac{\partial w}{\partial y}\right)^2 \\ \frac{\partial u}{\partial y} + \frac{\partial v}{\partial x} + \frac{\partial w}{\partial x}\frac{\partial w}{\partial y} \end{Bmatrix} \\ &+ \begin{bmatrix} D_{11} & D_{12} & D_{16} \\ D_{12} & D_{22} & D_{26} \\ D_{16} & D_{26} & D_{66} \end{bmatrix} \begin{Bmatrix} -\frac{\partial^2 w}{\partial x^2} \\ -\frac{\partial^2 w}{\partial y^2} \\ -2\frac{\partial^2 w}{\partial x \partial y} \end{Bmatrix} - \begin{Bmatrix} M^{\theta}_{xx} \\ M^{\theta}_{yy} \\ M^{\theta}_{xy} \end{Bmatrix} \end{aligned} \tag{4}$$

where the extensional, coupling, and bending stiffnesses are respectively defined by

$$\begin{bmatrix} A_{11} & A_{12} & A_{16} \\ A_{12} & A_{22} & A_{26} \\ A_{16} & A_{26} & A_{66} \end{bmatrix} = \int_{-h/2}^{h/2} \begin{bmatrix} Q_{11} & Q_{12} & Q_{16} \\ Q_{12} & Q_{22} & Q_{26} \\ Q_{16} & Q_{26} & Q_{66} \end{bmatrix} dz \tag{5a}$$

$$\begin{bmatrix} B_{11} & B_{12} & B_{16} \\ B_{12} & B_{22} & B_{26} \\ B_{16} & B_{26} & B_{66} \end{bmatrix} = \int_{-h/2}^{h/2} \begin{bmatrix} Q_{11} & Q_{12} & Q_{16} \\ Q_{12} & Q_{22} & Q_{26} \\ Q_{16} & Q_{26} & Q_{66} \end{bmatrix} z dz \tag{5b}$$

$$\begin{pmatrix} D_{11} & D_{12} & D_{16} \\ D_{12} & D_{22} & D_{26} \\ D_{16} & D_{26} & D_{66} \end{pmatrix} = \int_{-h/2}^{h/2} \begin{pmatrix} Q_{11} & Q_{12} & Q_{16} \\ Q_{12} & Q_{22} & Q_{26} \\ Q_{16} & Q_{26} & Q_{66} \end{pmatrix} z^2 dz \tag{5c}$$

in which Q_{ij} are the stiffness coefficients associated with the material properties. The quantities N^{θ}_{xx}, N^{θ}_{yy}, and N^{θ}_{xy} are thermal stress resultants and M^{θ}_{xx}, M^{θ}_{yy}, and M^{θ}_{xy} are thermal moment resultants given by

$$\begin{Bmatrix} N^{\theta}_{xx} \\ N^{\theta}_{yy} \\ N^{\theta}_{xy} \end{Bmatrix} = \int_{-h/2}^{h/2} \begin{pmatrix} Q_{11} & Q_{12} & Q_{16} \\ Q_{12} & Q_{22} & Q_{26} \\ Q_{16} & Q_{26} & Q_{66} \end{pmatrix} \begin{Bmatrix} \alpha_{xx}(\theta, z) \\ \alpha_{yy}(\theta, z) \\ \alpha_{xy}(\theta, z) \end{Bmatrix} \theta(z) dz \tag{6}$$

$$\begin{Bmatrix} M^{\theta}_{xx} \\ M^{\theta}_{yy} \\ M^{\theta}_{xy} \end{Bmatrix} = \int_{-h/2}^{h/2} \begin{pmatrix} Q_{11} & Q_{12} & Q_{16} \\ Q_{12} & Q_{22} & Q_{26} \\ Q_{16} & Q_{26} & Q_{66} \end{pmatrix} \begin{Bmatrix} \alpha_{xx}(\theta, z) \\ \alpha_{yy}(\theta, z) \\ \alpha_{xy}(\theta, z) \end{Bmatrix} \theta(z) z dz \tag{7}$$

3. Governing equations

To quantify the stress and displacement distributions of the plate due to thermo-mechanical loads, equilibrium and compatibility equations must be solved simultaneously. The former relates the axial forces to the out-of-plane displacement of the plate whereas the latter relates the internal membrane forces due to large deformations to the out-of-plane displacement.

The force resultants may be expressed by the stress function F as follows

$$\begin{Bmatrix} N_{xx} \\ N_{yy} \\ N_{xy} \end{Bmatrix} = \begin{Bmatrix} \frac{\partial^2 F}{\partial y^2} \\ \frac{\partial^2 F}{\partial x^2} \\ -\frac{\partial^2 F}{\partial x \partial y} \end{Bmatrix} \tag{8}$$

By rearranging Eq. (3) and using Eq. (8), the middle plane strains can then be written

as

$$\left\{\begin{array}{c} \frac{\partial u}{\partial x}+\frac{1}{2}\left(\frac{\partial w}{\partial x}\right)^2 \\ \frac{\partial v}{\partial y}+\frac{1}{2}\left(\frac{\partial w}{\partial y}\right)^2 \\ \frac{\partial u}{\partial y}+\frac{\partial v}{\partial x}+\frac{\partial w}{\partial x}\frac{\partial w}{\partial y} \end{array}\right\} = \left(\begin{array}{ccc} a_{11} & a_{12} & a_{16} \\ a_{12} & a_{22} & a_{26} \\ a_{16} & a_{26} & a_{66} \end{array}\right)\left\{\begin{array}{c} \frac{\partial^2 F}{\partial y^2} \\ \frac{\partial^2 F}{\partial x^2} \\ -\frac{\partial^2 F}{\partial x \partial y} \end{array}\right\} + \left(\begin{array}{ccc} b_{11} & b_{12} & b_{16} \\ b_{12} & b_{22} & b_{26} \\ b_{16} & b_{26} & b_{66} \end{array}\right)\left\{\begin{array}{c} \frac{\partial^2 w}{\partial x^2} \\ \frac{\partial^2 w}{\partial y^2} \\ 2\frac{\partial^2 w}{\partial x \partial y} \end{array}\right\} + \left(\begin{array}{ccc} a_{11} & a_{12} & a_{16} \\ a_{12} & a_{22} & a_{26} \\ a_{16} & a_{26} & a_{66} \end{array}\right)\left\{\begin{array}{c} N_{xx}^{\theta} \\ N_{yy}^{\theta} \\ N_{xy}^{\theta} \end{array}\right\} \tag{9}$$

in which the coefficients a_{ij} and b_{ij} are related to the stiffness coefficients A_{ij} and B_{ij} as defined in the following

$$\left(\begin{array}{ccc} a_{11} & a_{12} & a_{16} \\ a_{12} & a_{22} & a_{26} \\ a_{16} & a_{26} & a_{66} \end{array}\right) = \left(\begin{array}{ccc} A_{11} & A_{12} & A_{16} \\ A_{12} & A_{22} & A_{26} \\ A_{16} & A_{26} & A_{66} \end{array}\right)^{-1} \tag{10a}$$

$$\left(\begin{array}{ccc} b_{11} & b_{12} & b_{16} \\ b_{12} & b_{22} & b_{26} \\ b_{16} & b_{26} & b_{66} \end{array}\right) = \left(\begin{array}{ccc} A_{11} & A_{12} & A_{16} \\ A_{12} & A_{22} & A_{26} \\ A_{16} & A_{26} & A_{66} \end{array}\right)^{-1}\left(\begin{array}{ccc} B_{11} & B_{12} & B_{16} \\ B_{12} & B_{22} & B_{26} \\ B_{16} & B_{26} & B_{66} \end{array}\right) \tag{10b}$$

Substituting Eqs. (8) and (9) into the strain compatibility equation [16] leads to the following nonlinear equation:

$$\begin{aligned} &a_{22}\frac{\partial^4 F}{\partial x^4}-(a_{26}+a_{26})\frac{\partial^4 F}{\partial x^3 \partial y}+(2a_{12}+a_{66})\frac{\partial^4 F}{\partial x^2 y^2}-2a_{16}\frac{\partial^4 F}{\partial x \partial y^3}+a_{11}\frac{\partial^4 F}{\partial y^4}-\left(\frac{\partial^2 w}{\partial x \partial y}\right)^2 \\ &+\frac{\partial^2 w}{\partial x^2}\frac{\partial^2 w}{\partial y^2}+b_{12}\frac{\partial^4 w}{\partial x^4}+(2b_{26}-b_{16})\frac{\partial^4 w}{\partial x^3 \partial y}+(b_{11}+b_{22}-2b_{66})\frac{\partial^4 w}{\partial x^2 \partial y^2} \\ &+(2b_{16}-b_{26})\frac{\partial^4 w}{\partial x \partial y^3}+b_{12}\frac{\partial^4 w}{\partial y^4}=-a_{12}\frac{\partial^2 N_{xx}^{\theta}}{\partial x^2}+a_{16}\frac{\partial^2 N_{xx}^{\theta}}{\partial x \partial y}-a_{11}\frac{\partial^2 N_{xx}^{\theta}}{\partial y^2} \\ &\quad -a_{22}\frac{\partial^2 N_{yy}^{\theta}}{\partial x^2}+a_{26}\frac{\partial^2 N_{yy}^{\theta}}{\partial x \partial y}-a_{12}\frac{\partial^2 N_{yy}^{\theta}}{\partial y^2}-a_{26}\frac{\partial^2 N_{xy}^{\theta}}{\partial x^2}+a_{66}\frac{\partial^2 N_{xy}^{\theta}}{\partial x \partial y}-a_{16}\frac{\partial^2 N_{xy}^{\theta}}{\partial y^2} \end{aligned} \tag{11}$$

It can be seen that the effect of material nonlinearity is reflected in the coefficients a_{ij} and b_{ij} introduced in Eqs. (10).

To establish the compatibility equation, the moment resultants (9) are rewritten as

$$\begin{Bmatrix} M_{xx} \\ M_{yy} \\ M_{xy} \end{Bmatrix} = \begin{pmatrix} c_{11} & c_{12} & c_{16} \\ c_{12} & c_{22} & c_{26} \\ c_{16} & c_{26} & c_{66} \end{pmatrix} \begin{Bmatrix} \frac{\partial^2 F}{\partial y^2} \\ \frac{\partial^2 F}{\partial x^2} \\ -\frac{\partial^2 F}{\partial x \partial y} \end{Bmatrix} + \begin{pmatrix} d_{11} & d_{12} & d_{16} \\ d_{12} & d_{22} & d_{26} \\ d_{16} & d_{26} & d_{66} \end{pmatrix} \begin{Bmatrix} -\frac{\partial^2 w}{\partial x^2} \\ -\frac{\partial^2 w}{\partial y^2} \\ -2\frac{\partial^2 w}{\partial x \partial y} \end{Bmatrix} + \begin{pmatrix} c_{11} & c_{12} & c_{16} \\ c_{12} & c_{22} & c_{26} \\ c_{16} & c_{26} & c_{66} \end{pmatrix} \begin{Bmatrix} N^{\theta}_{xx} \\ N^{\theta}_{yy} \\ N^{\theta}_{xy} \end{Bmatrix} - \begin{Bmatrix} M^{\theta}_{xx} \\ M^{\theta}_{yy} \\ M^{\theta}_{xy} \end{Bmatrix} \tag{12}$$

where the coefficient c_{ij} and d_{ij} are related to the stiffness coefficients A_{ij}, B_{ij}, and D_{ij} as follows

$$\begin{pmatrix} c_{11} & c_{12} & c_{16} \\ c_{12} & c_{22} & c_{26} \\ c_{16} & c_{26} & c_{66} \end{pmatrix} = \begin{pmatrix} B_{11} & B_{12} & B_{16} \\ B_{12} & B_{22} & B_{26} \\ B_{16} & B_{26} & B_{66} \end{pmatrix} \begin{pmatrix} A_{11} & A_{12} & A_{16} \\ A_{12} & A_{22} & A_{26} \\ A_{16} & A_{26} & A_{66} \end{pmatrix}^{-1} \tag{13a}$$

$$\begin{aligned} &\begin{pmatrix} d_{11} & d_{12} & d_{16} \\ d_{12} & d_{22} & d_{26} \\ d_{16} & d_{26} & d_{66} \end{pmatrix} \\ &= \begin{pmatrix} D_{11} & D_{12} & D_{16} \\ D_{12} & D_{22} & D_{26} \\ D_{16} & D_{26} & D_{66} \end{pmatrix} \\ &\quad - \begin{pmatrix} B_{11} & B_{12} & B_{16} \\ B_{12} & B_{22} & B_{26} \\ B_{16} & B_{26} & B_{66} \end{pmatrix} \begin{pmatrix} A_{11} & A_{12} & A_{16} \\ A_{12} & A_{22} & A_{26} \\ A_{16} & A_{26} & A_{66} \end{pmatrix}^{-1} \begin{pmatrix} B_{11} & B_{12} & B_{16} \\ B_{12} & B_{22} & B_{26} \\ B_{16} & B_{26} & B_{66} \end{pmatrix} \end{aligned} \tag{13b}$$

The above matrices also represent the temperature-dependent material behaviour. Upon substitution of Eq. (12) into the equilibrium equation written in terms of the resultants

[16], the other nonlinear equation is established

$$
\begin{aligned}
&d_{11}\frac{\partial^4 w}{\partial x^4} + 2(d_{16}+d_{16})\frac{\partial^4 w}{\partial x^3 \partial y} + 2(d_{12}+2d_{66})\frac{\partial^4 w}{\partial x^2 y^2} + 4d_{26}\frac{\partial^4 w}{\partial x \partial y^3} + d_{22}\frac{\partial^4 w}{\partial y^4} \\
&- \frac{\partial^2 F}{\partial y^2}\frac{\partial^2 w}{\partial x^2} + 2\frac{\partial^2 F}{\partial x \partial y}\frac{\partial^2 w}{\partial x \partial y} - \frac{\partial^2 F}{\partial x^2}\frac{\partial^2 w}{\partial y^2} - c_{12}\frac{\partial^4 F}{\partial x^4} - (2c_{26}-c_{16})\frac{\partial^4 F}{\partial x^3 \partial y} \\
&- (c_{11}+c_{22}-2c_{66})\frac{\partial^4 F}{\partial x^2 y^2} - (2c_{16}-c_{26})\frac{\partial^4 F}{\partial x \partial y^3} - c_{12}\frac{\partial^4 F}{\partial y^4} = q + c_{11}\frac{\partial^2 N^{\theta}_{xx}}{\partial x^2} \\
&\quad + c_{12}\frac{\partial^2 N^{\theta}_{xx}}{\partial y^2} + 2c_{16}\frac{\partial^2 N^{\theta}_{xx}}{\partial x \partial y} + c_{12}\frac{\partial^2 N^{\theta}_{yy}}{\partial x^2} + c_{22}\frac{\partial^2 N^{\theta}_{yy}}{\partial y^2} + 2c_{26}\frac{\partial^2 N^{\theta}_{yy}}{\partial x \partial y} \\
&\quad + c_{16}\frac{\partial^2 N^{\theta}_{xy}}{\partial x^2} + c_{26}\frac{\partial^2 N^{\theta}_{xy}}{\partial y^2} + 2c_{66}\frac{\partial^2 N^{\theta}_{xy}}{\partial x \partial y} - \frac{\partial^2 M^{\theta}_{xx}}{\partial x^2} - \frac{\partial^2 M^{\theta}_{yy}}{\partial y^2} - 2\frac{\partial^2 M^{\theta}_{xy}}{\partial x \partial y}
\end{aligned}
\tag{14}
$$

where q represents the transverse mechanical load. The differential equations (11) and (14) are used in the next section to determine the out-of-plane displacement of the rectangular plate. The most common way of solving such equations is to use trigonometric functions. In terms of how the support conditions are specified, sine and/or cosine series solutions might be considered.

4. Solution method

In this study, two types of support conditions are assumed. The in-plane displacements are:

i. restrained to lateral translation, while the out-of-plane displacement is zero along the plate boundaries and rotations are free. In this case, TMA typically develops at large out-of-plane displacements, anchored by restraint to lateral translation at the boundaries as shown in Figure 2a. This type of BC is referred to as an 'immovable edge condition'.

ii. unrestrained against lateral translation, while the out-of-plane displacement is zero along the plate boundaries and rotations are free. In plates with such constraints undergoing large displacements, a degree of TMA can still occur. A feature of this mechanism is the appearance of a "compressive ring" in the plate as a manifestation of compressive membrane action in the outer regions of the plate which provides restraint to TMA occurring in the central region of the plate,

not dissimilar to the relatively rigid ring surrounding a trampoline. These features are shown schematically in Figure 2b. This BC is referred to as a 'free edge condition' in this paper in contrast to the immovable edge condition.

The aforementioned BCs are reasonable limiting cases bracketing the conditions that may be found in real structural frames. To fulfil the BCs, the following series expressions are assumed. The out-of-plane displacement is expanded in a double Fourier series as follows

$$w(x,y) = \sum_{m=1}^{\infty}\sum_{n=1}^{\infty} w_{mn} S_{mn} \tag{15}$$

where $S_{mn} = \sin(\bar{m}x)\sin(\bar{n}y)$ with $\bar{m} = m\pi/a$ and $\bar{n} = n\pi/b$. The thermal force and moment resultants can also be taken in the same form

$$\begin{Bmatrix} N^{\theta}_{xx}(x,y) \\ N^{\theta}_{yy}(x,y) \\ M^{\theta}_{xx}(x,y) \\ M^{\theta}_{yy}(x,y) \end{Bmatrix} = \sum_{m=1}^{\infty}\sum_{n=1}^{\infty} \begin{Bmatrix} N^{\theta}_{mnxx} \\ N^{\theta}_{mnyy} \\ M^{\theta}_{mnxx} \\ M^{\theta}_{mnyy} \end{Bmatrix} S_{mn} \tag{16}$$

where the coefficients are calculated by performing the Fourier integration as follows

$$\begin{Bmatrix} N^{\theta}_{mnxx} \\ N^{\theta}_{mnyy} \\ M^{\theta}_{mnxx} \\ M^{\theta}_{mnyy} \end{Bmatrix} = \frac{4\left[-1+(-1)^m\right]\left[-1+(-1)^n\right]}{mn\pi^2} \begin{Bmatrix} N^{\theta}_{xx} \\ N^{\theta}_{yy} \\ M^{\theta}_{xx} \\ M^{\theta}_{yy} \end{Bmatrix} \tag{17}$$

Note that, in the case of a laminated plate, N^{θ}_{xy}, M^{θ}_{xy}, Q_{16}, Q_{26} are zero.

Different transverse mechanical loading conditions can be considered by expressing the quantity q in a double Fourier series as

$$q(x,y) = \sum_{m=1}^{\infty}\sum_{n=1}^{\infty} q_{mn} S_{mn} \tag{18}$$

where the coefficient of the series is given by

$$q_{mn} = \frac{4}{ab}\int_0^a \int_0^b q(x,y) S_{mn} dy dx \tag{19}$$

The following loading conditions are then derived:

For uniformly distributed load (UDL) of magnitude q:

$$q_{mn} = \frac{4\left[-1+(-1)^m\right]\left[-1+(-1)^n\right]}{mn\pi^2}q \tag{20}$$

For sinusoidal loading of magnitude q where $m = n = 1$:

$$q_{mn} = q \tag{21}$$

For point load of q applied at coordinates (x_0,y_0):

$$q_{mn} = \frac{4q_0}{ab}\sin\frac{m\pi x_0}{a}\sin\frac{n\pi y_0}{b} \tag{22}$$

For the Airy stress function an expression satisfying the stress-free edge case (for free edge case) and undeformed edges case (for immovable case) may then be taken as

$$F(x,y) = \frac{P_x y^2}{2bh} + \frac{P_y x^2}{2ah} + \sum_{m=1}^{\infty}\sum_{n=1}^{\infty} F_{mn}S_{mn} \tag{23}$$

where P_x and P_y are equivalent reaction loads at the plate boundaries. In the case of immovable edge condition, such loads can be obtained using the following expressions for the elongation of the plate in the x and y directions

$$\int_0^a \frac{\partial u}{\partial x}dx = \int_0^a \left(a_{11}\frac{\partial^2 F}{\partial y^2} + a_{12}\frac{\partial^2 F}{\partial x^2} + b_{11}\frac{\partial^2 w}{\partial x^2} + b_{12}\frac{\partial^2 w}{\partial y^2} + a_{11}N_{xx}^{\theta} + a_{12}N_{yy}^{\theta} - \frac{1}{2}\left(\frac{\partial w}{\partial x}\right)^2 \right) dx \tag{24a}$$

$$\int_0^b \frac{\partial v}{\partial y}dy = \int_0^b \left(a_{12}\frac{\partial^2 F}{\partial y^2} + a_{22}\frac{\partial^2 F}{\partial x^2} + b_{12}\frac{\partial^2 w}{\partial x^2} + b_{22}\frac{\partial^2 w}{\partial y^2} + a_{12}N_{xx}^{\theta} + a_{22}N_{yy}^{\theta} - \frac{1}{2}\left(\frac{\partial w}{\partial y}\right)^2 \right) dy \tag{24b}$$

where setting the edge displacements to zero after substituting Eqs. (15) and (23) into Eqs. (24) and performing the integration, yields the following expressions for the reaction loads

$$P_x = \frac{bh\left(a_{22}\bar{m}^2 - a_{12}\bar{n}^2\right)}{8\left(a_{11}a_{22} - a_{12}^2\right)} w_{mn}^2 + \frac{[-1+(-1)^m][-1+(-1)^n]\, bh\bar{n}^2}{mn\pi^2} F_{mn} + \frac{bh[-1+(-1)^m][-1+(-1)^n]\left[(a_{12}b_{12} - a_{22}b_{11})\bar{m}^2 + (a_{12}b_{22} - a_{22}b_{12})\bar{n}^2\right]}{mn\pi^2\left(a_{11}a_{22} - a_{12}^2\right)} w_{mn} - bhN_{xx}^{\theta} \tag{25a}$$

$$P_y = \frac{ah\left(a_{11}\bar{n}^2 - a_{12}\bar{m}^2\right)}{8\left(a_{11}a_{22} - a_{12}^2\right)} w_{mn}^2 + \frac{[-1+(-1)^m][-1+(-1)^n]\, ah\bar{m}^2}{mn\pi^2} F_{mn} + \frac{ah[-1+(-1)^m][-1+(-1)^n]\left[(a_{11}b_{12} - a_{12}b_{11})\bar{m}^2 + (a_{11}b_{22} - a_{12}b_{12})\bar{n}^2\right]}{mn\pi^2\left(a_{11}a_{22} - a_{12}^2\right)} w_{mn} - ahN_{yy}^{\theta} \tag{25b}$$

In contrast, when the free edge condition is imposed, such reaction loads are zero at the plate boundaries and the following expressions can then be obtained for the in-plane displacements

$$u = \sum_{m=1}^{\infty}\sum_{n=1}^{\infty}\left[-\frac{\bar{m}^2}{4} w_{mn}^2\left(x + \frac{\sin 2\bar{m}x}{2\bar{m}}\right)\sin^2\bar{n}y + \frac{b_{11}\bar{m}^2 + b_{12}\bar{n}^2}{\bar{m}} w_{mn}\cos\bar{m}x\sin\bar{n}y + \frac{a_{12}\bar{m}^2 + a_{11}\bar{n}^2}{\bar{m}} F_{mn}\cos\bar{m}x\sin\bar{n}y + aa_{11}N_{xx}^{\theta} + aa_{12}N_{yy}^{\theta}\right] \tag{26a}$$

$$v = \sum_{m=1}^{\infty}\sum_{n=1}^{\infty}\left[-\frac{\bar{n}^2}{4} w_{mn}^2\sin^2\bar{m}x\left(y + \frac{\sin 2\bar{n}y}{2\bar{n}}\right) + \frac{b_{12}\bar{m}^2 + b_{22}\bar{n}^2}{\bar{n}} w_{mn}\sin\bar{m}x\cos\bar{n}y + \frac{a_{22}\bar{m}^2 + a_{12}\bar{n}^2}{\bar{n}} F_{mn}\sin\bar{m}x\cos\bar{n}y + ba_{12}N_{xx}^{\theta} + ba_{22}N_{yy}^{\theta}\right] \tag{26b}$$

It is clear that the coefficients of the in-plane displacements are also temperature-dependent. Considering the expressions (15)-(23) into the governing equations (11) and (14), for a rectangular plate with temperature-dependent material properties the compatibility and equilibrium equations are established as

$$\begin{aligned}&\left[a_{22}\bar{m}^4 + (2a_{12} + a_{66})\bar{m}^2\bar{n}^2 + a_{11}\bar{n}^4\right] F_{mn}S_{mn} - \bar{m}^2\bar{n}^2 w_{mn}^2\left(C_{mn}^2 - S_{mn}^2\right)\\ &+ \left[(b_{11} + b_{22} - 2b_{66})\bar{m}^2\bar{n}^2 + b_{12}\bar{m}^4 + b_{12}\bar{n}^4\right] w_{mn}S_{mn}\\ &- \left[\left(a_{12}N_{mnxx}^{\theta} + a_{22}N_{mnyy}^{\theta}\right)\bar{m}^2 + \left(a_{11}N_{mnxx}^{\theta} + a_{12}N_{mnyy}^{\theta}\right)\bar{n}^2\right] S_{mn} = 0\end{aligned} \tag{27}$$

$$
\begin{aligned}
&\left[d_{11}\bar{m}^4 + (2d_{12} + 4d_{66})\bar{m}^2\bar{n}^2 + d_{22}\bar{n}^4\right] w_{mn}S_{mn} \\
&\quad - \left[c_{12}\bar{m}^4 + (c_{11} + c_{22} - 2c_{66})\bar{m}^2\bar{n}^2 + c_{12}\bar{n}^4\right] F_{mn}S_{mn} \\
&\quad + \left(\frac{P_x\bar{m}^2}{bh} + \frac{P_y\bar{n}^2}{ah}\right) w_{mn}S_{mn} - 2\bar{m}^2\bar{n}^2F_{mn}w_{mn}\left(S_{mn}^2 - C_{mn}^2\right) \\
&\quad + \left[\left(c_{11}N_{mnxx}^{\theta} + c_{12}N_{mnyy}^{\theta}\right)\bar{m}^2 + \left(c_{12}N_{mnxx}^{\theta} + c_{22}N_{mnyy}^{\theta}\right)\bar{n}^2\right] S_{mn} \\
&\quad - \left(\bar{m}^2M_{mnxx}^{\theta} + \bar{n}^2M_{mnyy}^{\theta}\right) S_{mn} - q_{mn}S_{mn} = 0
\end{aligned}
\tag{28}
$$

where $C_{mn} = \cos(\bar{m}x)\cos(\bar{n}y)$. Using the expansion theorem [17], the stress function coefficient F_{mn} is obtained as a function of the unknown coefficient w_{mn}

$$
\begin{aligned}
F_{mn} = \frac{1}{(a_{22}\bar{m}^4 + (2a_{12} + a_{66})\bar{m}^2\bar{n}^2 + a_{11}\bar{n}^4)} &\left[4\bar{m}^2\bar{n}^2H_{mn}w_{mn}^2\right. \\
&- \left[(b_{11} + b_{22} - 2b_{66})\bar{m}^2\bar{n}^2 + b_{12}\bar{m}^4 + b_{12}\bar{n}^4\right] w_{mn} \\
&\left. + \left[\left(a_{12}N_{mnxx}^{\theta} + a_{22}N_{mnyy}^{\theta}\right)\bar{m}^2 + \left(a_{11}N_{mnxx}^{\theta} + a_{12}N_{mnyy}^{\theta}\right)\bar{n}^2\right]\right]
\end{aligned}
\tag{29}
$$

where

$$
H_{mn} = \frac{-1 + 2(-1)^m + 2(-1)^n - (-1)^{3m} - (-1)^{3n} - 3(-1)^{m+n} + (-1)^{3m+n} + (-1)^{m+3n}}{3mn\pi^2}
\tag{30}
$$

In a similar way, the following load-deflection equation is derived from the equilibrium equation (28)

$$
\varsigma_1 w_{mn} + \varsigma_2 F_{mn} + \varsigma_3 F_{mn}w_{mn} + \varsigma_4 = 0
\tag{31}
$$

where

$$
\varsigma_1 = \frac{P_x\bar{m}^2}{bh} + \frac{P_y\bar{n}^2}{ah} + d_{11}\bar{m}^4 + (2d_{12} + 4d_{66})\bar{m}^2\bar{n}^2 + d_{22}\bar{n}^4 \tag{32a}
$$

$$
\varsigma_2 = -c_{12}\bar{m}^4 - (c_{11} + c_{22} - 2c_{66})\bar{m}^2\bar{n}^2 - c_{12}\bar{n}^4 \tag{32b}
$$

$$
\varsigma_3 = 8\bar{m}^2\bar{n}^2H_{mn} \tag{32c}
$$

$$
\begin{aligned}
\varsigma_4 = &\left[\left(c_{11}N_{mnxx}^{\theta} + c_{12}N_{mnyy}^{\theta}\right)\bar{m}^2 + \left(c_{12}N_{mnxx}^{\theta} + c_{22}N_{mnyy}^{\theta}\right)\bar{n}^2\right] \\
&- \left(\bar{m}^2M_{mnxx}^{\theta} + \bar{n}^2M_{mnyy}^{\theta}\right) - q_{mn}
\end{aligned}
\tag{32d}
$$

It should be noted that the required computational time is minimised by neglecting higher order terms in the nonlinear governing equations due to their low contribution to the final solutions [17, 18].

Once the material and geometric parameters are known, the coefficient w_{mn} can be readily obtained by substituting the stress function from Eq. (29) into (31). Having resolved the load-deflection equation (31), the out-of-plane displacement of the plate can be accurately calculated for an adequate number of series terms. To achieve reasonable accuracy a limited number of terms are retained in the series solutions. This depends on the specified support conditions for the plate and is discussed in the next section.

4.1. Temperature profile

In the present paper, attention has been restricted to the nonlinear heating of plates through the thickness. As such, the temperature is constant in the plane of the plate. There are various methods for determining such a one-dimensional temperature profile. In the case of plate structures under fire conditions, a popular method is carrying out an FE heat transfer analysis. Hence, in this study, temperature distributions through the thickness were calculated using a Fortran FE code [19]. A typical exponential time-temperature relation for the gas temperature in a compartment is given by [1]

$$\theta(t) = \theta_0 + (\theta_{max} - \theta_0)\left(1 - \mathrm{e}^{-\eta t}\right) \tag{33}$$

where θ_0 is the ambient temperature (20°C), θ_{max} is the maximum temperature, η is a parameter controlling the 'rate of heating', and t is an artificial time variable considered to only provide a sensitivity analysis to the current computation. Since the aim is examining the effect of different non-uniform temperature profiles on the plate response, steady-state conditions are assumed. The FE heat transfer analysis was carried out for a plate of 0.07 m thickness under two different fire scenarios:

i. A "short hot" exponential fire representing a high heating rate ($\eta = 0.005$) with a maximum temperature of 1000°C when the bottom surface of the plate was heated for 1,200 s.

ii. A "Long cool" exponential fire representing a low heating rate ($\eta = 0.001$) with a maximum temperature of 600°C when the bottom surface of the plate was heated for 21,600 s.

Figures 3 and 4 illustrate the time-temperature curves and through the thickness temperature distributions for the short hot fire and long cool fire, respectively. Both figures show the typical temperature distribution for plate structures under a one directional heat source which causes the temperature to decay exponentially over the thickness. As expected, the top surface is the coolest as it is the furthest from the heat source at the bottom surface. This approach allows the study of two extreme cases of high and low rates of heating. The two temperature profiles chosen from the FE heat transfer analysis are shown in Figure 5. An analysis was then carried out for the particular cases of heating rate parameter η fitting the chosen fire time-temperature curves. The generalised expression was obtained as

$$\theta(z) = \theta_0 + (\theta_{max} - \theta_0)\mathrm{e}^{\mu\left(\frac{z}{h}-\frac{1}{2}\right)} \tag{34}$$

where the rate of change in the temperature is governed by the dimensionless parameter μ. Clearly the thermal curvature is greater when μ is higher. The temperature distribution is constant for $\mu = 0$. For the chosen fire scenarios the corresponding temperature profiles are achieved by the following expressions

$$\text{Low heating rate} : \theta(z) = 70.81 + 225.87\ \mathrm{e}^{3\left(\frac{z}{h}-\frac{1}{2}\right)} \tag{35a}$$

$$\text{High heating rate} : \theta(z) = 34.18 + 571.16\ \mathrm{e}^{4.4\left(\frac{z}{h}-\frac{1}{2}\right)} \tag{35b}$$

The assumed non-uniform temperature profiles can be used to study the structural behaviour of plates under most likely fire scenarios with different rates of heating.

4.2. Temperature-dependency of material properties

In order to determine the actual load-carrying capacity of plate structures, variation in mechanical and thermal properties of the plate at elevated temperatures should be addressed in the analysis. This requires appropriate expressions in the formulation to account for the nonlinear behaviour of material properties at elevated temperatures. Eurocode [8] provides empirical data for the reduction in structural steel and concrete stiffness at elevated temperatures as two common constructional materials, whereas Australian Standard gives the following expressions for the elastic modulus of structural steel [20]

$$E(\theta, z) = E_0 \begin{cases} 1 + \frac{\theta}{2000 \ln \frac{\theta}{1100}}, & 0°\text{C} < \theta \leq 600\,°\text{C} \\ \frac{690\left(1 - \frac{\theta}{1000}\right)}{\theta - 53.5}, & 600\,°\text{C} \leq \theta \leq 1000\,°\text{C} \end{cases} \tag{36}$$

and for the elastic modulus of concrete [21]

$$E(\theta, z) = E_0 \begin{cases} 1, & 0°\text{C} \leq \theta \leq 60\,°\text{C} \\ \frac{720 - \theta}{660}, & 60\,°\text{C} \leq \theta \leq 720\,°\text{C} \end{cases} \tag{37}$$

where E_0 is the elastic modulus of the corresponding material at ambient temperature and E_θ is its corresponding modulus at elevated temperature. In Figure 6, acquired data from both standards are plotted for comparison. As can be seen, suitable curves are constructed to have the best fit to the series of data points provided in the Eurocode for reduction in elastic modulus of steel and concrete at elevated temperatures. The corresponding mathematical expressions are

$$\text{For steel} : E(\theta, z) = E_0 \mathrm{e}^{-\left(\frac{\theta - 54.6}{523.8}\right)^2} \tag{38a}$$

$$\text{For concrete} : E(\theta, z) = E_0 \mathrm{e}^{-\left(\frac{\theta - 52.06}{532}\right)^2} \tag{38b}$$

It should be noted that no expression is reported in both standards for the variation of the coefficient of thermal expansion for steel and concrete with temperature. Nevertheless, the first derivative of the thermal elongation given in Eurocode [8] is used to obtain expressions representing the reduction of the coefficient of thermal expansion at elevated temperatures for steel

$$\alpha(\theta, z) = \begin{cases} 1.2 \times 10^{-5} + 0.8 \times 10^{-8}\theta, & 20°\text{C} < \theta \leq 750\,°\text{C} \\ 0, & 750\,°\text{C} < \theta \leq 860\,°\text{C} \\ 2 \times 10^{-5}, & 860°\text{C} < \theta \leq 1200\,°\text{C} \end{cases} \tag{39}$$

and normal weight concrete

$$\alpha(\theta, z) = \begin{cases} 9 \times 10^{-6} + 6.9 \times 10^{-11}\theta^2, & 20°\text{C} \leq \theta \leq 700\,°\text{C} \\ 0, & 700\,°\text{C} < \theta \leq 1200\,°\text{C} \end{cases} \tag{40}$$

where α_0 is the coefficient of thermal expansion of the corresponding material at ambient temperature and α_θ is its counterpart at elevated temperature. The coefficient of thermal expansion increases smoothly for structural steel and dramatically for normal weight concrete with temperature. It drops to zero as for steel it undergoes phase

change from ferrite-pearlite microstructure to a high temperature phase called austenite and for concrete it is due to a phase change arising from loss of chemically bound water at high temperatures. It is worth mentioning here that the coefficient of thermal expansion for lightweight concrete is constant and equal to $8 \times 10^{-6}(1/^{\circ}\mathrm{C})$.

There is another expression reported by Touloukian [22] for taking into account the temperature-dependency of material properties (TDMP). That is,

$$P(\theta) = P_0\left(P_{-1}\theta^{-1} + 1 + P_1\theta + P_2\theta^2 + P_3\theta^3\right) \tag{41}$$

where P denotes a material property such as elastic modulus, coefficient of thermal expansion or thermal conductivity, and P_0, P_{-1}, P_1, P_2, and P_3 are coefficients of environment temperature θ in Kelvin and are unique for each material. Typical values for these coefficients can be found in Reddy and Chin [23]. Expression (41) is commonly used for analysis of FG plates, in which the material properties vary continuously throughout the thickness direction according to the volume fraction of constituents given by either a power-law distribution [24, 25] or an exponential function [26]. For instance, the material property P is expressed as

$$P(\theta, z) = (P_t - P_b)\left(\frac{1}{2} - \frac{z}{h}\right)^{\lambda} + P_b \tag{42}$$

where $\lambda(\geq 0)$ is the volume fraction index and P_t and P_b denote the material properties of the top and bottom surfaces of the plate, respectively.

Note that, this study will not account for the dependence of temperature on the Poisson's ratio since this effect is considered negligible, hence in the following analysis it is assumed equal to 0.3.

5. Results and discussion

Numerical results are presented in this section for thin rectangular plates having immovable or free BCs subjected to UDL and a non-uniform through-depth temperature distribution. As stated earlier, the TDMP is taken into account in the analysis, and as a result of that, both geometrical and material nonlinearities are included in the model. The dimensionless parameters used are listed in Table 1.

To assess the accuracy and performance of the proposed method, several numerical examples are presented.

5.1. Plate under UDL

First, results from comparison studies are presented for square plates at uniform ambient temperature. In Table 2, results of the dimensionless central deflection for a square plate with immovable and free BCs under UDL of 100 are listed. The plate has a thickness-span ratio of 0.001 and elasticity modulus of 205 GPa. The results obtained using the method presented are compared with results derived by an analytical method based on the von Kármán plate theory [27] as well as with a finite element method (FEM) solution [28]. The present results agree very well with FE solution with almost zero error for the free BC case and about 3% error for the immovable BC case.

In Figure 7, load-deflection curves of an immovable FG square plate with thickness-span ratio of 0.05 are shown for different volume fraction indices. The lower surface of the plate is assumed to be metal (aluminum) rich while the upper surface is assumed to be pure ceramic (alumina). The elastic modulus is taken as 70 GPa and 380 GPa for aluminum and alumina, respectively. The UDL is non-dimensionalised using the aluminum's elastic modulus. It can be seen that the results obtained using the method presented are in very good agreement with those obtained from an analytical solution based on the classical plate theory [29].

5.2. Plate under thermal loading

For this loading case, the results are validated for elevated temperatures. An immovable square plate with a thickness-span ratio of 0.02, elasticity modulus of 40 GPa and coefficient of thermal expansion of 8×10^{-6} (1/°C) is considered. A temperature distribution causing an equivalent thermal gradient of 5000°C/m and an equivalent thermal expansion of 200°C is chosen. The non-dimensional central deflection using the method presented is compared with the solutions of ABAQUS FE package [30] and an analytical method [30] in Table 3. Comparing the results obtained by these three methods reveals that the result predicted by the present method is in very good agreement with the one predicted by the FE analysis, indicating this is the more accurate solution for determining the deflection in a plate subjected to thermal gradients.

5.3. Plate under thermo-mechanical loading

As the first example for this loading case, in Figure 8 the dimensionless central deflection of an FG square plate is compared with deflections obtained from an analytical solution based on a higher-order shear deformation plate theory [31]. The plate is made of a mixture of silicon nitride and stainless steel with a volume fraction index of 2 and thickness-span ratio of 0.1. It is subjected to UDL in a thermal environmental condition at 300 K. The TDMP is also considered in the analysis and material properties are graded through the thickness of the plate according to the power-law distribution introduced in Eq. (42). The values of the coefficients of temperature in Eq. (41) are listed in Table 4 [23]. It is clearly seen that very good agreement is attained for this loading case.

In the following, the nonlinear response of rectangular plates to short hot heating and long cool heating is studied. Due to inherent complexities in the problem studied, computational time increases when large number of terms are considered in the series solutions. To overcome this drawback, optimal number of terms are determined for both BC cases. In Figures 9 and 10 convergence of the series solutions is studied for the nonlinear central deflection of a square plate subjected to dimensionless UDL of 200 and short hot and long cool heating regimes for the immovable and free BCs, respectively. The plate has thickness-span ratio of 0.007, elasticity modulus of 27 GPa and coefficient of thermal expansion of 9×10^{-6} (1/°C). The results are presented with and without considering the TDMP. It is found that for the free BC case, one term might be sufficient to achieve reasonable accuracy to the actual solutions, however, for the immovable case, three series terms are required.

To investigate the effect of the plate geometry, different aspect and thickness-span ratios are considered in Tables 5 and 6. As can be seen, both ratios have a nonlinear influence on the plate deflection. The central deflection for the plate with free edge condition is computed using only one term in the series solutions, while for the immovable plate it is computed using three terms. This is justified through convergence studies and resulted in a considerable saving in computation time without losing accuracy. Figures 11 and 12 show the variation of non-dimensional UDL parameter with the central deflection for immovable and free BCs, respectively, with and without considering the

TDMP. It can be seen that the effect of TDMP is significant in both boundary cases, in particular in the case of free edge condition.

The effect of the TDMP on the plate response is also highlighted by plotting dimensionless membrane forces (N_{yy}) in Figure 13 for an immovable plate and in Figure 14 for a plate with free edge condition. Results are monitored in four different locations across the plate span for both heating regimes. The plate has the same material properties and geometry as mentioned above and is subjected to the same UDL. In the case of long cool heating, it can be observed from the graphs that the difference of the results with and without considering the TDMP are not significant. However, in the case of short hot heating such difference is found to be notable. This is mainly due to the fact that at high temperatures the material strength starts to drop faster than at lower temperatures.

Figure 15 illustrates the vector plots of all dimensionless principal membrane forces for a square plate with free edge condition subjected to UDL of 100 and the two heating regimes when TDMP is considered. The lengths of the vectors are proportional to their magnitudes. As observed in Figure 14, the magnitude of the membrane forces are higher in the case of short hot fire than that of in the long cool fire. This can also be seen in Figure 15. The reason for this is that higher gradients in the short hot fire creates larger curvatures, thereby increasing the contribution of membrane forces in carrying the load. However, lower deflections in the long cool fire mean that the contribution of bending resistance is relatively greater, therefore membrane forces are lower. The figure clearly shows TMA in the plate with tensile membrane stresses in the central zone and compressive membrane stresses around perimeter of the plate. The existence of both tension zone in the middle and compression zone around perimeter of the plate leads to the formation of a “compressive ring” which is highlighted with blue arrows in the figures. This phenomenon has been recognised as an important load-carrying mechanism of “last resort” in the full-scale fire tests at Cardington in the UK [32].

6. Conclusions

A geometrically and materially nonlinear analysis was developed to study the nonlinear response of rectangular plates to non-uniform thermal gradients across the thickness of the plate. The temperature-dependency of the plate's material properties was considered in the analysis to account for the variation in material strength at elevated temperatures. Since the BCs of the problem play the key role in choosing the type of series solutions, no general solution was provided for rectangular plates having arbitrary BCs. Hence, two common types of support conditions were considered; displacements were assumed restrained or unrestrained against lateral translations, while the out-of-plane displacement was fixed and rotations were assumed free. The main conclusions are:

i. The accuracy of the results for both BC cases are acceptable and the solutions can be used as trial functions for hybrid-type FEMs. In the case of free edge condition, only one term in the series solutions was sufficient for obtaining reasonably accurate response, in contrast to the immovable case in which three series terms were required in the calculations. It should be noted that to quantify the evolution of the compression ring in the tensile membrane action (for the free BC case), five series terms were used.

ii. The consideration of thermal gradients in the plate that represents a wide range of fire exposures provided insights into improving the fire performance of plate structures. The methodology developed is very useful for benchmarking FE codes developed for thermo-mechanical simulations of shell elements. The short hot fire exposure typically led to large gradients and a low mean temperature, while the long cool fire exposure was vice versa.

iii. The results have shown that despite the larger area under the long cool fire time-temperature curve, which traditionally represented the fire severity, the effect of the short hot fire on the plate behaviour is more pronounced. The effect of the TDMP also was most prominent during the short hot heating.

iv. Although the numerical analysis is confined to the case of rectangular plates under two fire conditions based upon likely fires that could occur, the application of the method presented to other arbitrary non-uniform in-depth thermal gradients considering the TDMP is straightforward.

In order to fully investigate the effect of the compressive ring in improving the fire performance of plate structures, further investigation is required to quantify the "anatomy" of the compressive ring.

Acknowledgement

The authors gratefully acknowledge funding support from the Edinburgh Research Partnership in Engineering (ERPe).

References

[1] Usmani, A., Chung, Y., Torero, J.L.. How did the WTC towers collapse: A new theory. Fire Safety Journal 2003;38(6):501–533.

[2] Barut, A., Madenci, E., Tessler, A.. Nonlinear thermoelastic analysis of composite panels under non-uniform temperature distribution. International Journal of Solids and Structures 2000;37(27):3681–3713.

[3] Jin, L.J., Oh, I.K., Lee, I., Yeom, C.H.. Thermal post-buckling behavior of patched laminated panels under uniform and non-uniform temperature distributions. Composite Structures 2002;55(2):137–145.

[4] Na, K.S., Kim, J.H.. Nonlinear bending response of functionally graded plates under thermal loads. Journal of Thermal Stresses 2006;29(3):245–261.

[5] Sabik, A., Kreja, I.. Large thermo-elastic displacement and stability FEM analysis of multilayered plates and shells. Thin-Walled Structures 2013;71:119–133.

[6] Jeyaraj, P.. Buckling and free vibration behavior of an isotropic plate under nonuniform thermal load. International Journal of Structural Stability and Dynamics 2013;13(03).

[7] Salminen, M., Heinisuo, M.. Numerical analysis of thin steel plates loaded in shear at non-uniform elevated temperatures. Journal of Constructional Steel Research 2014;97:105–113.

[8] Eurocode, . EN 1993-1-2, Eurocode 3: Design of Steel Structures, Part 1-2: General rules - Structural fire design. 2005.

[9] Shukla, K., Nath, Y.. Nonlinear analysis of moderately thick laminated rectangular plates. Journal of Engineering Mechanics 2000;126(8):831–838.

[10] Woo, J., Meguid, S.. Nonlinear analysis of functionally graded plates and shallow shells. International Journal of Solids and structures 2001;38(42):7409–7421.

[11] Shen, H.S.. Thermal postbuckling behavior of shear deformable FGM plates with temperature-dependent properties. International Journal of Mechanical Sciences 2007;49(4):466–478.

[12] Li, S.R., Zhang, J.H., Zhao, Y.G.. Nonlinear thermomechanical post-buckling of circular FGM plate with geometric imperfection. Thin-walled Structures 2007;45(5):528–536.

[13] Sepahi, O., Forouzan, M., Malekzadeh, P.. Large deflection analysis of thermo-mechanical loaded annular FGM plates on nonlinear elastic foundation via DQM. Composite Structures 2010;92(10):2369–2378.

[14] Khazaeinejad, P., Usmani, A., Laghrouche, O.. Transient thermoelastic analysis of plates by hybrid-Trefftz method. In: 11th International Conference on Vibration Problems (ICOVP-2013). 2013,.

[15] Khazaeinejad, P., Usmani, A.. Analytical solutions for nonlinear response of plates under thermal loading. In: Proceedings of the 8th International Conference on Structures in Fire (SiF'14). 2014,.

[16] Timoshenko, S., Woinowsky-Krieger, S., Woinowsky-Krieger, S.. Theory of plates and shells; vol. 2. McGraw-hill New York; 1959.

[17] Khazaeinejad, P., Usmani, A., Laghrouche, O.. An analytical study of the nonlinear thermo-mechanical behaviour of thin isotropic rectangular plates. Computers & Structures 2014;141:1–8.

[18] Khazaeinejad, P., Usmani, A., Laghrouche, O.. Nonlinear stress analysis of plates under thermo-mechanical loads. In: Journal of Physics: Conference Series; vol. 382. IOP Publishing; 2012, p. 012022.

[19] Huang, H.C., Usmani, A.S.. Finite element analysis for heat transfer. Springer; 1994.

[20] Standards Australia, . Steel structures, AS4100. 1998.

[21] Standards Australia, . Concrete structures, AS3600. 2001.

[22] Touloukian, Y.. Thermophysical properties of high temperature solid materials. MacMillan; 1967.

[23] Reddy, J., Chin, C.. Thermomechanical analysis of functionally graded cylinders and plates. Journal of Thermal Stresses 1998;21(6):593–626.

[24] Najafizadeh, M., Mahdavian, M., Khazaeinejad, P.. Superposition buckling analysis of rectangular plates composed of functionally graded materials subjected to non-uniform distributed in-plane loading. Proceedings of the Institution of Mechanical Engineers, Part C: Journal of Mechanical Engineering Science 2010;224(11):2299–2307.

[25] Najafizadeh, M., Mohammadi, J., Khazaeinejad, P.. Vibration characteristics of functionally graded plates with non-ideal boundary conditions. Mechanics of Advanced Materials and Structures 2012;19(7):543–550.

[26] Khazaeinejad, P., Najafizadeh, M.. Mechanical buckling of cylindrical shells with varying material properties. Proceedings of the Institution of Mechanical Engineers, Part C: Journal of Mechanical Engineering Science 2010;224(8):1551–1557.

[27] Wang, D., El-Sheikh, A.. Large-deflection mathematical analysis of rectangular plates. Journal of Engineering Mechanics 2005;131(8):809–821.

[28] Reddy, J.N.. Mechanics of laminated composite plates and shells: Theory and analysis. CRC press; 2004.

[29] GhannadPour, S., Alinia, M.. Large deflection behavior of functionally graded plates under pressure loads. Composite Structures 2006;75(1):67–71.

[30] Usmani, A., Cameron, N.. Limit capacity of laterally restrained reinforced concrete floor slabs in fire. Cement and Concrete Composites 2004;26(2):127–140.

[31] Shen, H.S., Wang, Z.X.. Nonlinear bending of FGM plates subjected to combined loading and resting on elastic foundations. Composite Structures 2010;92(10):2517–2524.

[32] Usmani, A., Drysdale, D., Rotter, J., Sanad, A., Gillie, M., Lamont, S., et al. Behaviour of steel framed structures under fire conditions. Tech. Rep.; School of Civil and Environmental Engineering, The University of Edinburgh; 2000.

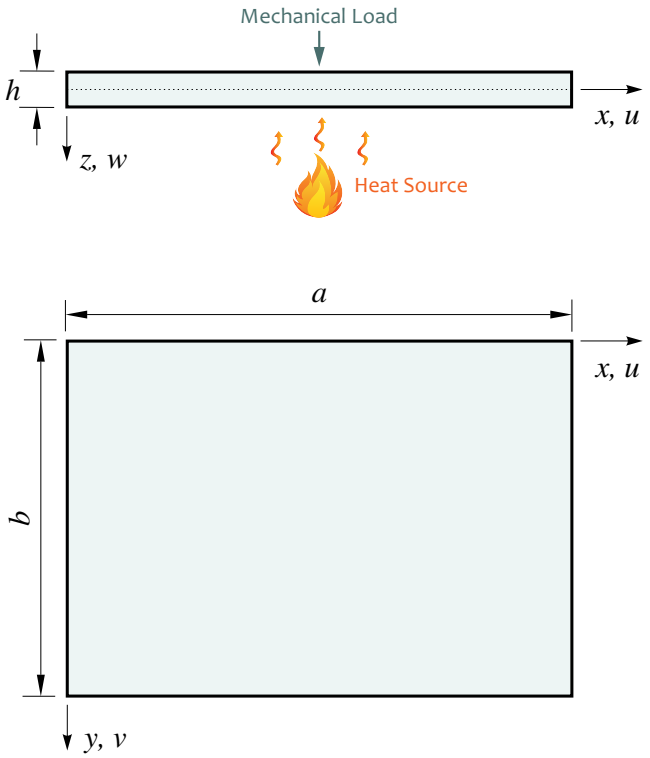

Figure 1: Configuration of a rectangular plate under a transverse mechanical load and a non-uniform thermal gradient caused by a heat source such as fire. For plate structures under fire conditions, interest lies mainly in the variation of temperature through the depth of the plate.

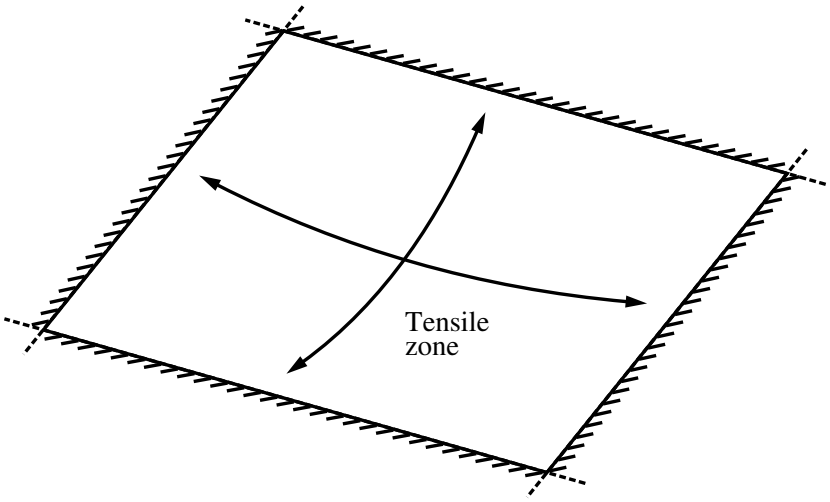

(a) Immovable edge condition

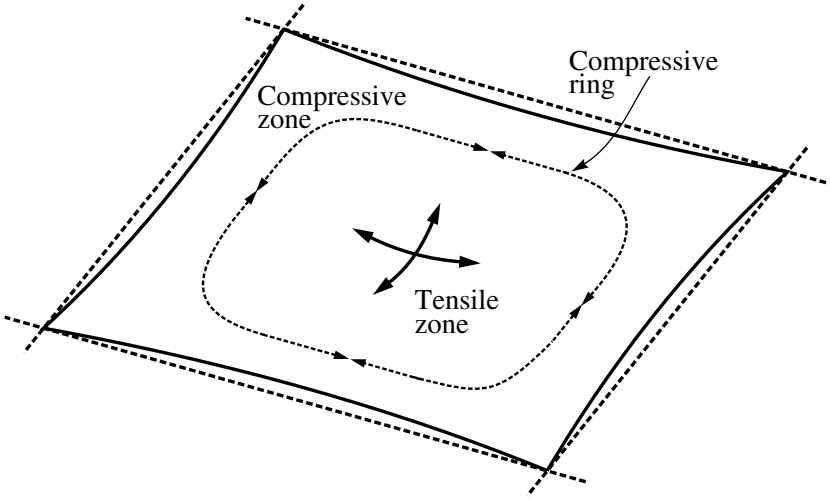

(b) Free edge condition

Figure 2: The schematic views of the BCs specified for the plate.

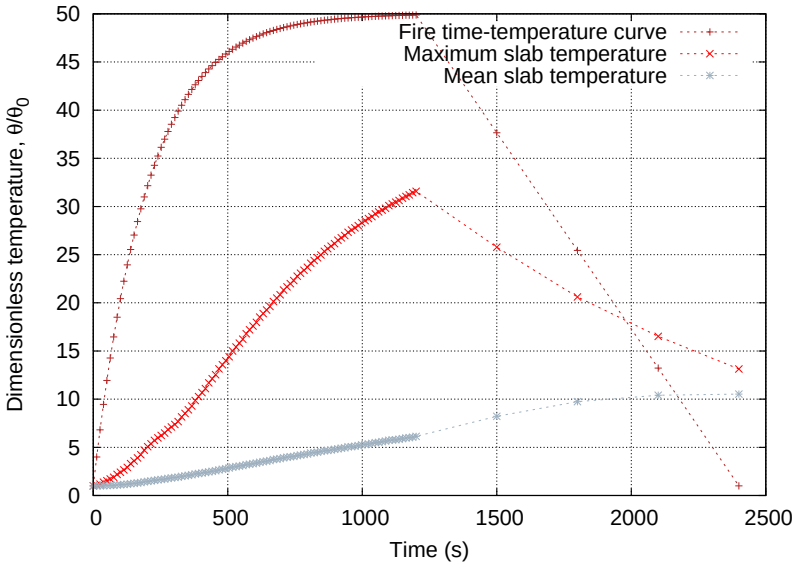

(a) Time-temperature curve

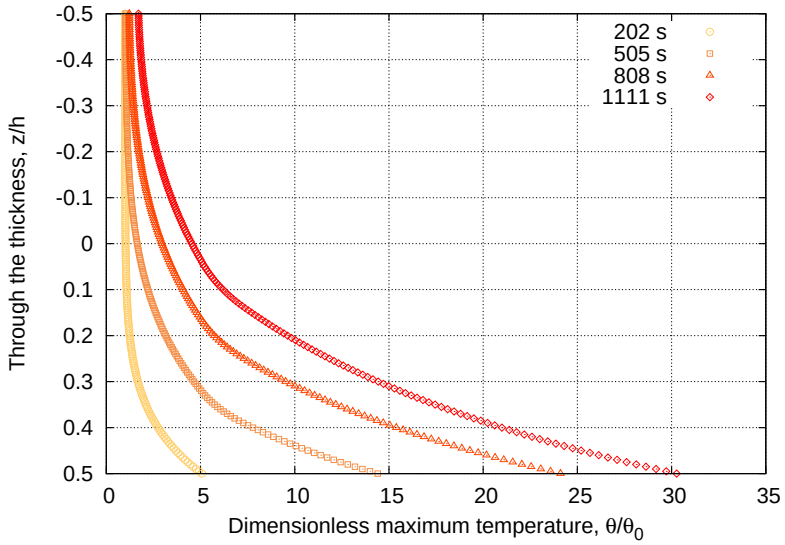

(b) Through-depth temperature

Figure 3: Time-temperature curve and through the thickness temperature distribution for the short hot exponential fire.

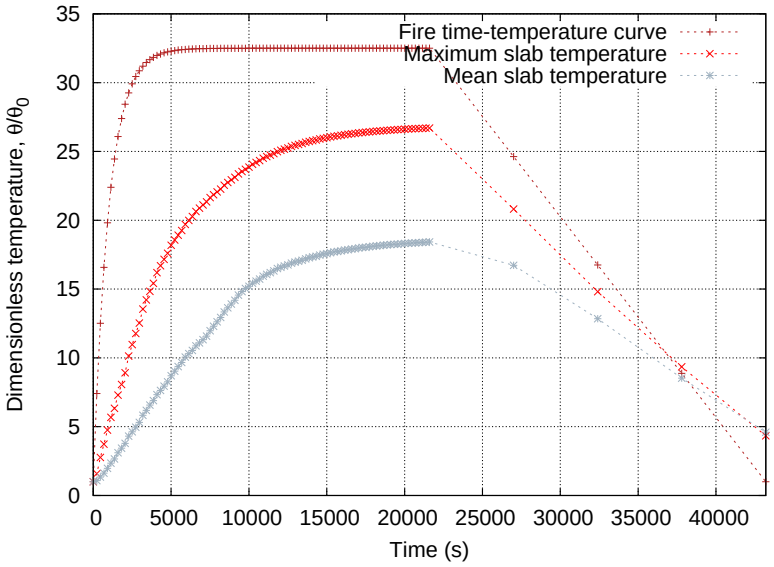

(a) Time-temperature curve

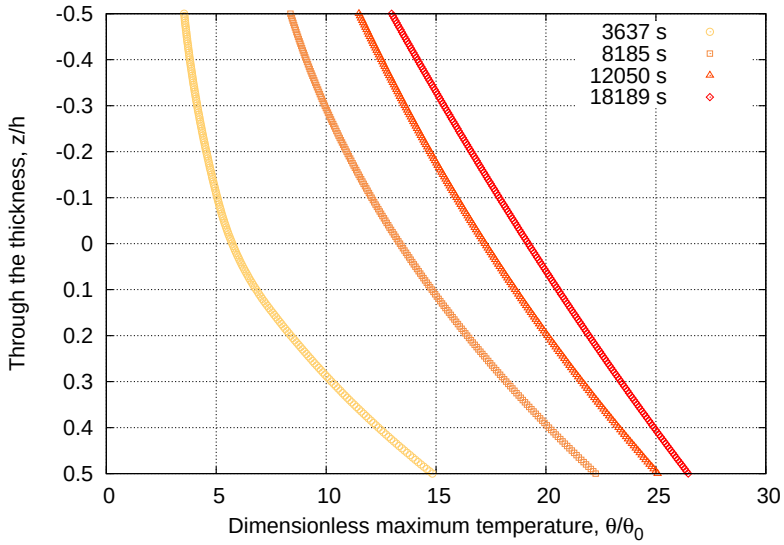

(b) Through-depth temperature

Figure 4: Time-temperature curve and through the thickness temperature distribution for the long cool exponential fire.

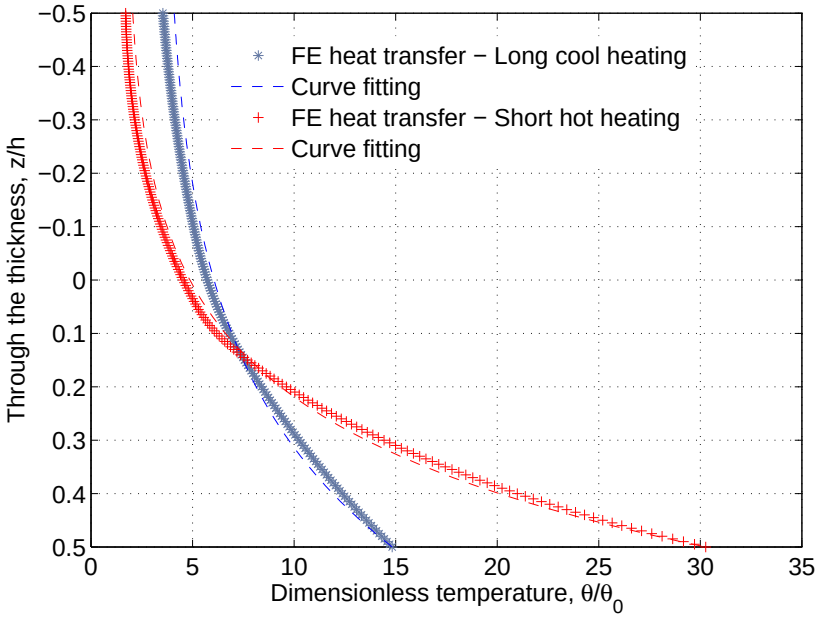

Figure 5: Non-uniform temperature distributions over the thickness of the plate using the FE heat transfer analysis. The assumed curve fitting functions correspond to the high and low rates of heating.

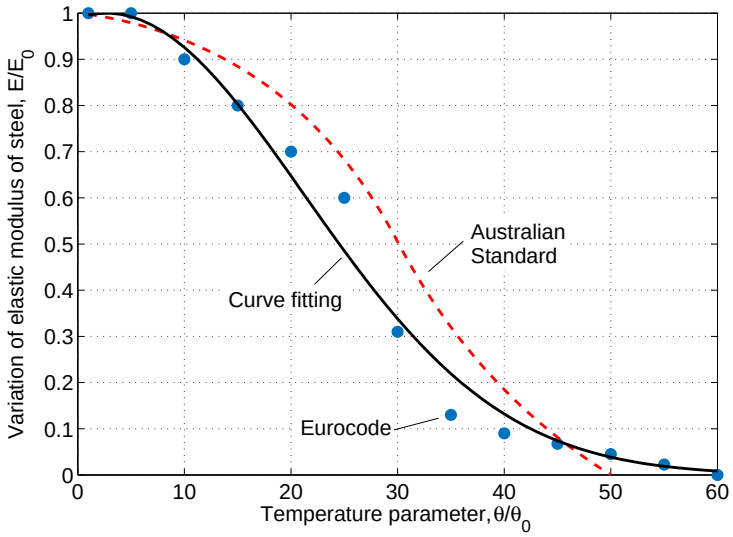

(a) Structural steel

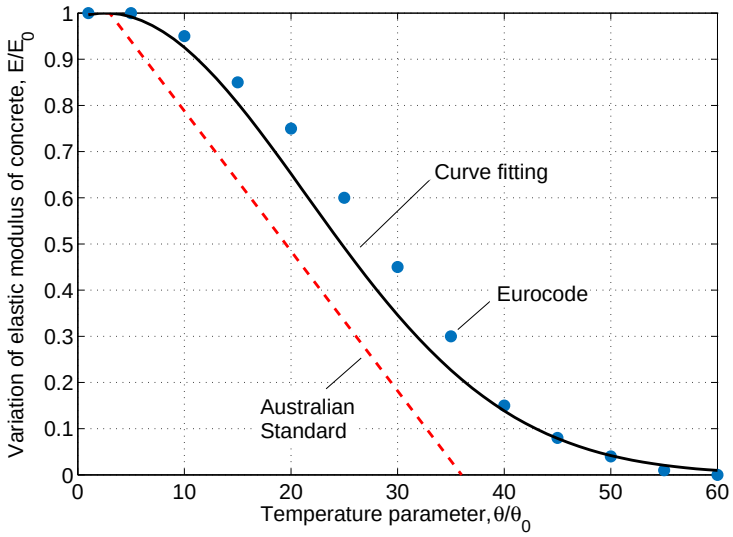

(b) Concrete

Figure 6: Degradation of elastic modulus at elevated temperatures. The elastic modulus rapidly decreases with temperature for both materials.

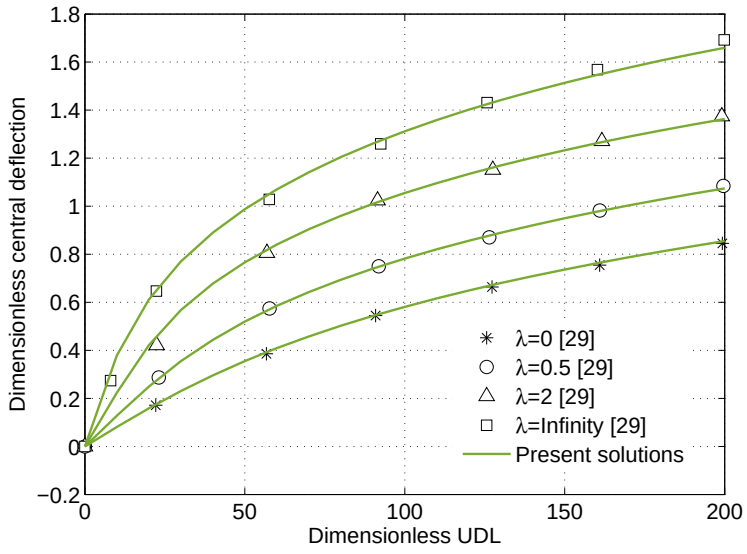

Figure 7: Dimensionless central deflection of an immovable FG square plate ($h/a = 0.05$) over a wide range of non-dimensional UDL. Results are obtained using three terms in the series solutions.

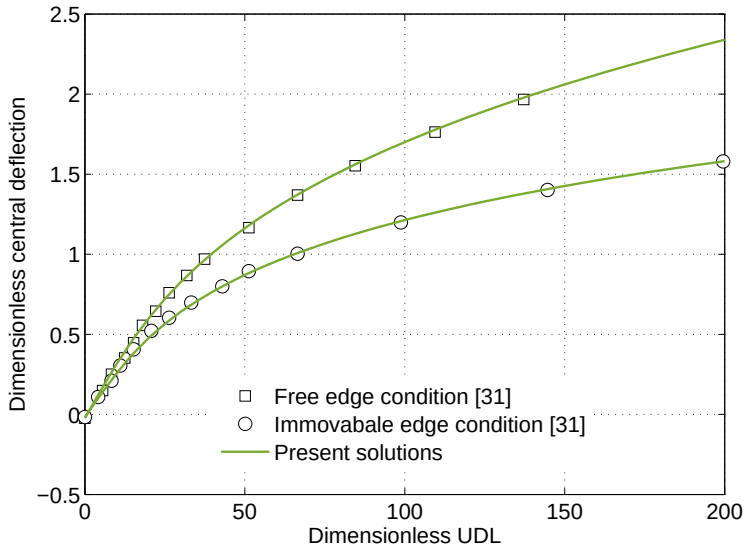

Figure 8: Dimensionless central deflection of an FG square plate ($h/a = 0.1$) having either immovable of free edge condition under thermal environmental condition and a wide range of non-dimensional UDL.

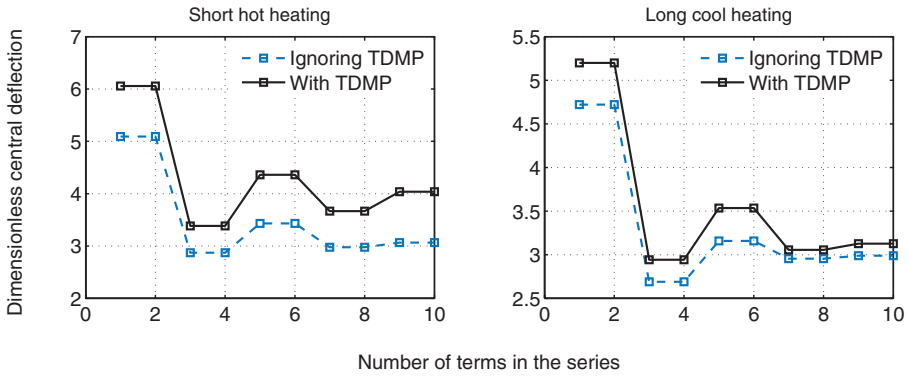

Figure 9: Convergence of the dimensionless nonlinear central deflection for an immovable square plate ($h/a = 0.007$) subjected to UDL (of 200) and two heating regimes and. The Effect of TDMP is considered when calculating the solutions.

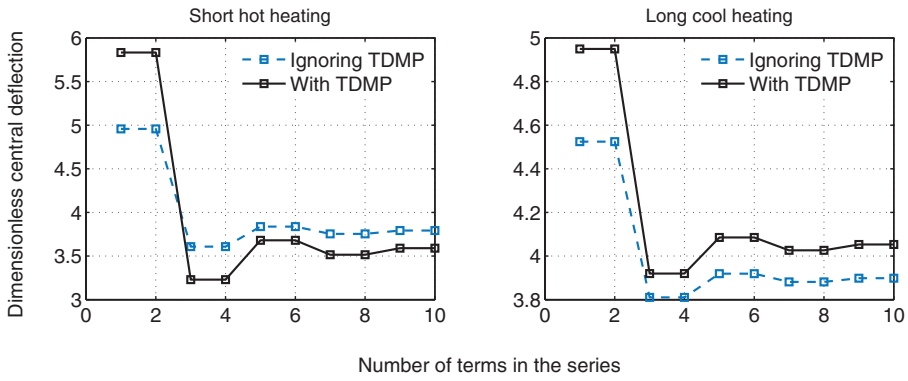

Figure 10: Convergence of the dimensionless nonlinear central deflection for a square plate ($h/a = 0.007$) with free edge condition subjected to UDL (of 200) and two heating regimes and. The Effect of TDMP is considered when calculating the solutions.

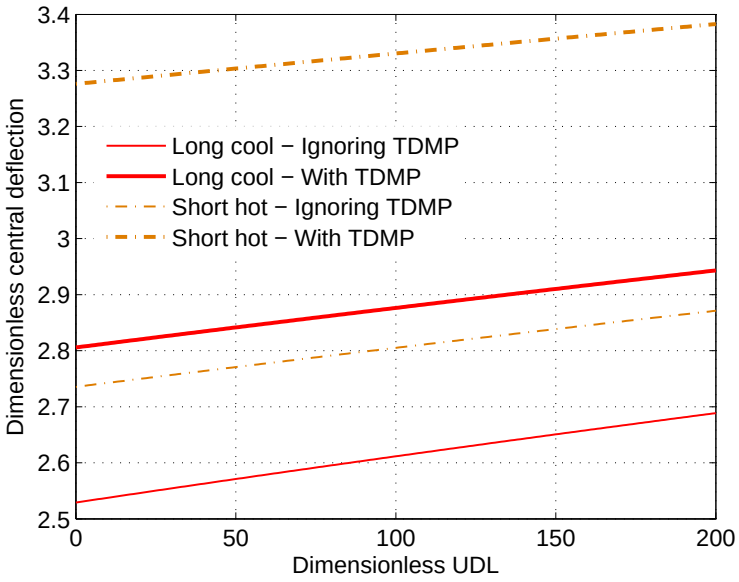

Figure 11: Dimensionless central deflection of an immovable square plate ($h/a = 0.007$) over a wide range of non-dimensional UDL. Results are obtained using three terms in the series solutions with and without considering the TDMP.

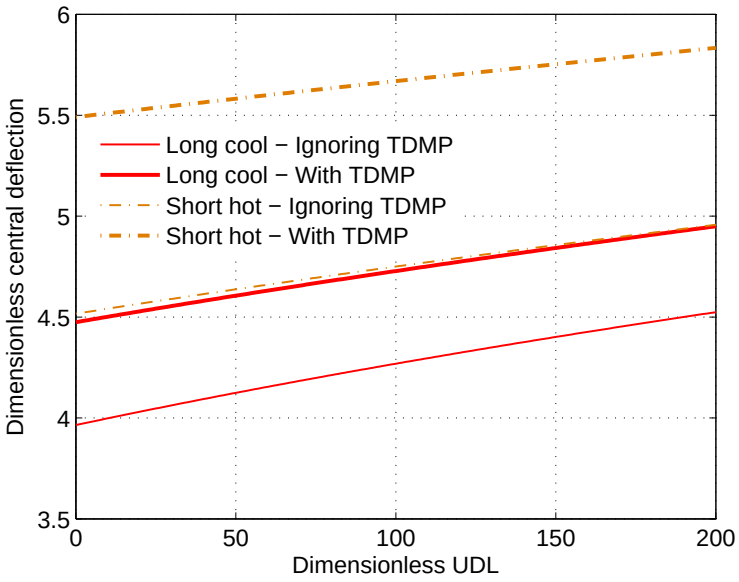

Figure 12: Dimensionless central deflection of a square plate ($h/a = 0.007$) with free edge condition over a wide range of non-dimensional UDL. Results are obtained using one term in the series solutions with and without considering the TDMP.

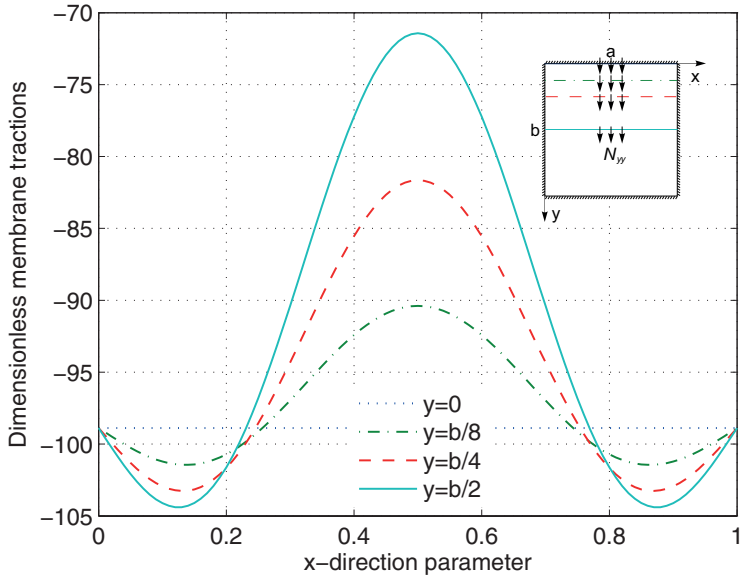

(a) Short hot fire

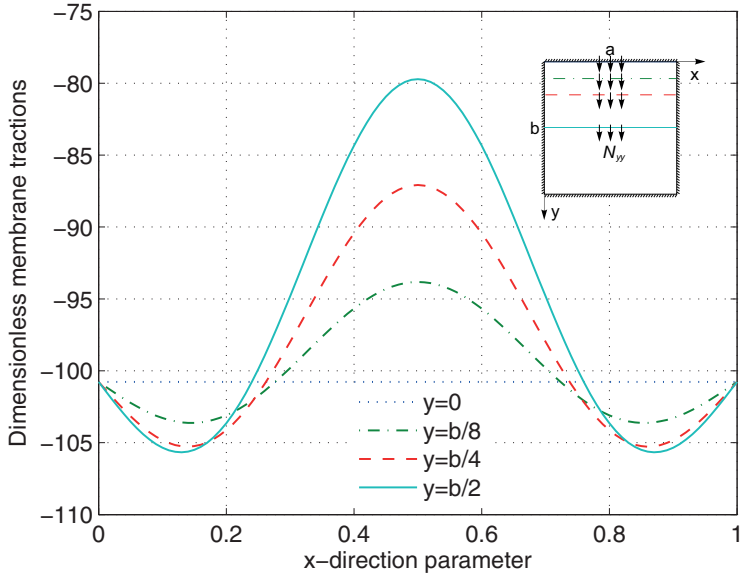

(b) Long cool fire

Figure 13: Dimensionless membrane forces (N_{yy}) for an immovable plate across its span. The plate is subjected to two heating regimes and UDL (of 200) while considering TDMP.

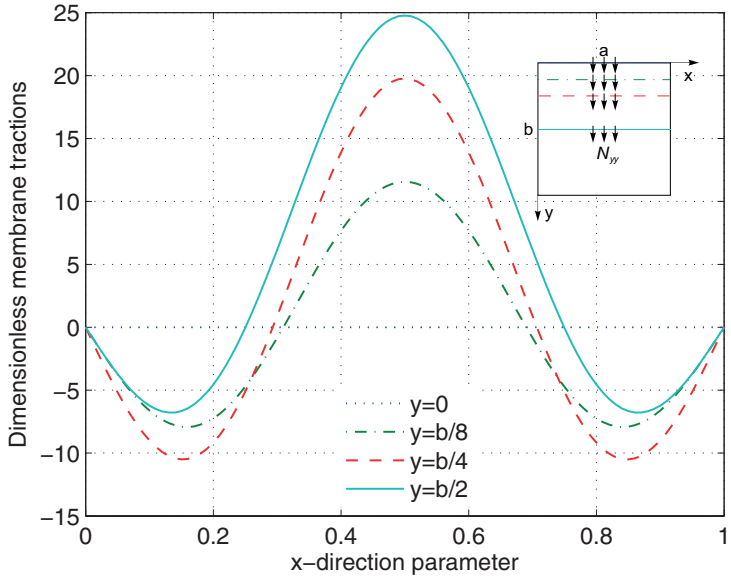

(a) Short hot fire

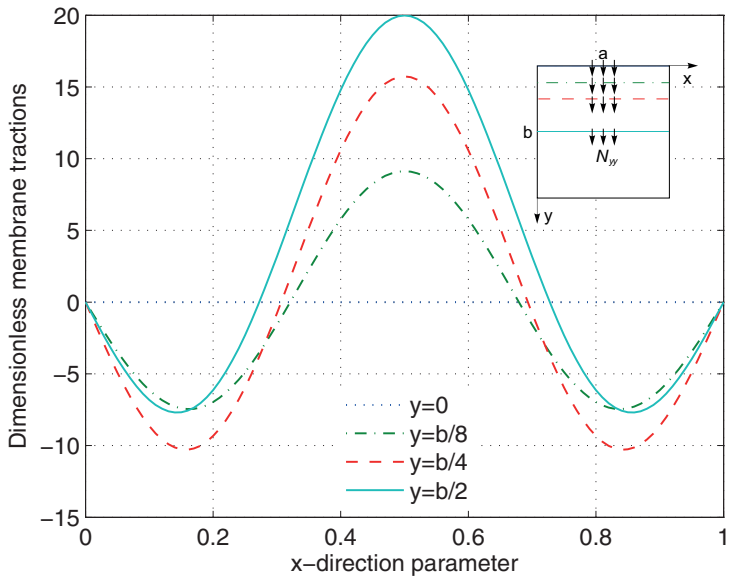

(b) Long cool fire

Figure 14: Dimensionless membrane forces (N_{yy}) for a plate with free edge condition across its span. The plate is subjected to two heating regimes and UDL (of 200) while considering the TDMP.

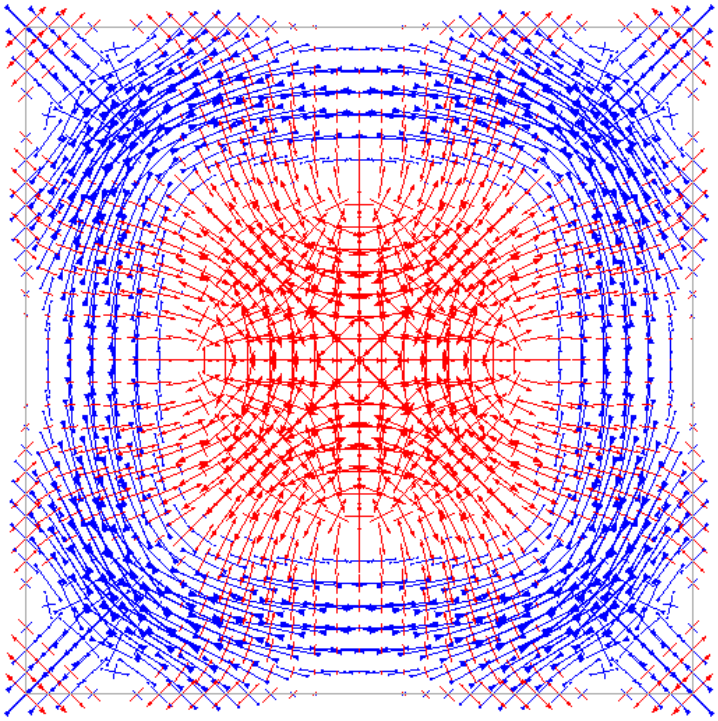

(a) Short hot fire

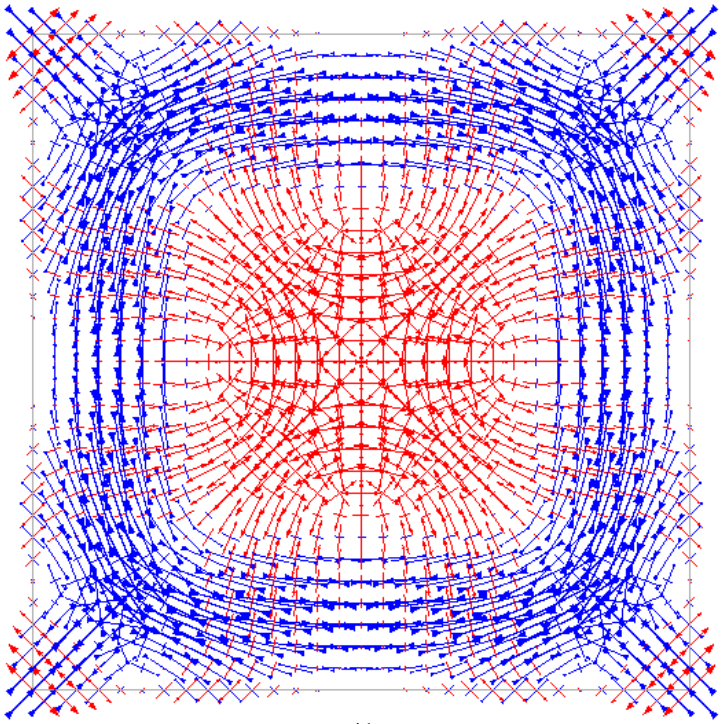

(b) Long cool fire

Figure 15: Representation of compressive ring for temperature-dependent plates under non-uniform heating. Blue arrows represent compressive stresses and the red ones represent tensile stresses.

Table 1: Definitions of dimensionless quantities

Description	Definition
Aspect ratio	a/b
Thickness-span ratio	h/a
Dimensionless central deflection	w/h
Dimensionless UDL	qa^4/E_0h^4
Dimensionless membrane force	Na^2/E_0h^3

Table 2: Comparison studies for dimensionless central deflection of a square plate ($h/a = 0.001$) having either immovable of free edge condition under UDL of 100

BC	Analytical method [27]	FEM [28]	Present solution	
Immovable	1.27 (6)*	–	1.312 (3)	1.321 (5)
Free	1.88 (6)	1.8827 (3)	1.883 (1)	1.777 (5)

*The digits in parentheses are the number of terms in the series taken for convergence.

Table 3: Comparison studies for dimensionless central deflections of an immovable square plate under thermal gradient

Solution method	Deflection	Number of series terms used
Analytical method [30]	1.48	1
ABAQUS [30]	1.36	–
Present solution	1.37	3

Table 4: Coefficients of temperature for the FG plate [23].

Materials	Quantity	Coefficients				
		P_0	P_{-1}	P_1	P_2	P_3
Silicon Nitride (Si_3N_4)	E	348.43×10^{9}	0	-3.070×10^{-4}	2.160×10^{-7}	-8.946×10^{-11}
	α	5.8723×10^{-6}	0	9.095×10^{-4}	0	0
Stainless Steel (SUS304)	E	201.04×10^{9}	0	3.079×10^{-4}	-6.534×10^{-7}	0
	α	12.330×10^{-6}	0	8.086×10^{-4}	0	0

Table 5: Effect of aspect and thickness-span ratios on the dimensionless central deflection of a plate under short hot heating and UDL of 200

Aspect ratio		Thickness-span ratio				
		0.005	0.007	0.008	0.01	0.015
Immovable edge condition						
1	Ignoring TDMP	3.907	2.871	2.554	2.107	1.713
	With TDMP	4.622	3.384	3.006	2.490	1.803
2	Ignoring TDMP	2.935	2.123	1.869	1.510	0.967
	With TDMP	3.494	2.535	2.235	1.815	1.240
3	Ignoring TDMP	1.277	0.937	0.830	0.677	0.418
	With TDMP	1.538	1.136	1.010	0.832	0.580
Free edge condition						
1	Ignoring TDMP	6.555	4.958	4.487	3.872	3.177
	With TDMP	7.771	5.834	5.252	4.475	3.562
2	Ignoring TDMP	10.010	7.219	6.338	5.094	3.423
	With TDMP	12.010	8.736	7.704	6.247	4.282
3	Ignoring TDMP	14.150	10.090	8.776	6.886	4.197
	With TDMP	17.120	12.390	10.880	8.718	5.688

Table 6: Effect of aspect and thickness-span ratios on the dimensionless central deflection of a plate under long cool heating and UDL of 200

Aspect ratio		Thickness-span ratio				
		0.005	0.007	0.008	0.01	0.015
Immovable edge condition						
1	Ignoring TDMP	3.646	2.689	2.397	1.965	1.774
	With TDMP	4.006	2.943	2.620	2.169	1.726
2	Ignoring TDMP	2.721	1.964	1.727	1.392	0.902
	With TDMP	3.003	2.169	1.909	1.544	0.990
3	Ignoring TDMP	1.166	0.850	0.751	0.609	0.338
	With TDMP	1.295	0.947	0.838	0.683	0.433
Free edge condition						
1	Ignoring TDMP	5.959	4.524	4.114	3.591	3.026
	With TDMP	6.570	4.950	4.478	3.866	3.188
2	Ignoring TDMP	8.980	6.378	5.557	4.403	2.888
	With TDMP	10.010	7.162	6.263	4.999	3.317
3	Ignoring TDMP	12.530	8.700	7.458	5.654	3.063
	With TDMP	14.080	9.915	8.577	6.646	3.897